Three-dimensional hierarchical nickel-based hydroxides and oxides microspheres and their electrochemical properties

Hui Liu, Xiaonan Dong, Congyue Duan, Xing Su, Zhenfeng Zhu

School of Materials Science and Engineering, Shaanxi University of Science and Technology, Xi'an 710021, People's Republic of China
E-mail: liuhui@sust.edu.cn

Published in Micro & Nano Letters; Received on 22nd May 2013; Revised on 30th July 2013; Accepted on 5th September 2013

Nickel hydroxides ($Ni(OH)_2$) with various morphologies, including flower-like, walnut-like and particle-aggregated microspheres, have been successfully synthesised by a surfactant-assisted microwave hydrothermal method. NiO microspheres have been obtained by calcining corresponding $Ni(OH)_2$ precursors at 400°C for 2 h. The products were characterised by X-ray diffraction, Fourier transform infrared spectroscopy, thermogravimetric analysis, scanning electron microscopy and transform electron microscopy. The electrochemical properties of the NiO microspheres with different morphologies were also investigated.

1. Introduction: Nickel hydroxide ($Ni(OH)_2$), one of the most important transition metal hydroxides, has attracted increasing attention as it is a unique cathode material, which can be widely used in many applications, such as power tools, portable electronics, electric vehicles, positive electrode active material and so on. [1]. Hexagonal layered $Ni(OH)_2$ has two polymorphs with α- and β-forms [2]. Mostly, the active materials of positive electrodes are β-$Ni(OH)_2$ because of its stability in a strong alkaline electrolyte and excellent reversibility. The as-calcined NiO has also aroused considerable attention because of its applications in areas such as chemical sensors, catalysis, fuel cell electrodes and dye-sensitised solar cells [3–5]. The overall performance of nickel cathodes depends on the microstructure, the textural characteristics and the crystallite size of the active material [6]. Thus, the design and synthesis of the morphology-controlled nickel-based nanocrystals have been intensively pursued, especially the organisation of nanostructured building blocks, such as nanoparticles, nanorods, nanowires, nanosheets and so on into three-dimensional (3D) ordered superstructures by bottom-up approaches has been an exciting research field [7–13]. Furthermore, developing a facile and environment-friendly route to produce 3D hierarchical micro/nanostructures is very important for nanoscience and synthetic chemistry.

Here, we report the synthesis of $Ni(OH)_2$ and NiO with various morphologies, including flower-like, walnut-like and particle-aggregated microspheres, by a surfactant-assisted microwave hydrothermal method. Polyethylene glycol (PEG) with different molecular weights and different filling ratios for the autoclave had an important effect on the formation of $Ni(OH)_2$ with different morphologies. The as-calcined NiO microspheres retain the same morphology as their $Ni(OH)_2$ precursors. Finally, we investigated the electrochemical properties of NiO microspheres with different morphologies.

2. Experimental: All the reagents were of analytical grade and were used without further purification.

2.1. Synthesis of flower-like microsphere precursor: In the experiment, 0.12 g PEG-20000 was dissolved in 5 ml deionised water to form a transparent solution. Then, 0.29 g $Ni(NO_3)_2 \cdot 6H_2O$ was added to the above solution under stirring, followed by the addition of 15 ml ethanol and 50 ml $CO(NH_2)_2$ solution. Then, 2 ml $NH_3 \cdot H_2O$ was added dropwise into the above solution to form a clear blue solution at pH ≃ 9. The final solution was transferred into a 100 ml Teflon-lined autoclave. Then, the autoclave was sealed and heated in an MDS-8 microwave hydrothermal system at 160°C for 0.5 h, then cooled to room temperature naturally. The resulting pale green slurry was rinsed with deionised water and absolute ethanol several times to remove soluble impurities. The precipitate was dried at 80°C in a vacuum oven for 12 h to obtain the sample S-1.

2.2. Synthesis of walnut-like and particles aggregated microspheres precursors: In the test, 0.6 g PEG-6000 was dissolved in 25 ml deionised water to form a transparent solution. Then, the $Ni(NO_3)_2 \cdot 6H_2O$ solution was added to the above solution under vigorous stirring, followed by an addition of 25 ml $CO(NH_2)_2$ solution to form a clear blue solution and then transferred into a 100 ml Teflon-lined autoclave, leaving the autoclave about half full. The autoclave was sealed and treated at 160°C for 30 min in an MDS-8 microwave hydrothermal system. After that the reaction was terminated and the autoclave was cooled to room temperature. The resulting pale green slurry was rinsed with deionised water and absolute ethanol several times to remove soluble impurities. The precipitate was dried at 80°C in a vacuum oven for 12 h to obtain the sample S-2. The procedure of sample S-3 was nearly same as S-2 except that the autoclave was filled in proportion to ¾.

2.3. Synthesis of NiO nanostructues: The as-obtained precursors were calcined in air at 400°C for 2 h to produce NiO nanostructures that preserved the precursors' morphology.

2.4. Characterisation: The crystalline phases of the products were characterised by using X-ray diffraction (XRD-D/max2200pc, Japan) with Cu Kα radiation of wavelength $\lambda = 0.15418$ nm. The Fourier transform infrared (FTIR) spectroscopy of the sample was conducted at room temperature with a KBr pellet on a VECTOR-70 (Bruker) spectrometer. The morphology of the products was characterised with a JSM-6700F field-emission scanning electron microscope operated at 5 kV and JEM 2010 transmission electron microscope operated at 200 kV. Thermogravimetric analysis was performed by a TG-DSC analyser (TGA 2050 thermogravimetric, DTG-60AH SHIMADZU, Japan).

2.5. Electrochemical test: Flower-like, walnut-like and particle-aggregated nickel oxide microspheres were mixed with ionic liquid [IL, 1-butyl-3-methylimidazolium bromide

(BmimBr)] to form three stable composite films, which were used to immobilise haemoglobin (Hb). The as-prepared composite electrodes (CPE) used NiO with flower-like, walnut-like and particle-aggregated microspherical architectures and were labelled as F-NiO/IL/Hb-CPE, W-NiO/IL/Hb-CPE and A-NiO/IL/Hb-CPE, respectively. All electrochemical measurements were carried out with a CHI660B electrochemical workstation (Shanghai Chenhua Co.) controlled by a microcomputer with CHI660 software. A three-electrode system was used, where an Ag/AgCl (3 M KCl) electrode served as the reference electrode, a platinum wire electrode as the auxiliary electrode and a modified CPE as the working electrode. Cyclic voltammetric measurements were conducted in an unstirred 30 ml electrochemical cell at 25°C.

3. Results and discussion: Fig. 1 shows the XRD patterns of the as-prepared precursors and corresponding calcined products at different temperatures. Except for the weak diffraction peak at $2\theta = 14.68°$ corresponding to the hexagonal α-$Ni(OH)_2$, all the other peaks of sample S-1 (curve a) ascribed to the hexagonal phase of β-$Ni(OH)_2$ (JCPDS Card No. 14-117) because of the addition of ammonium [14]. When the system pH was less than 9.5, the particle's structure was neither α-$Ni(OH)_2$ nor β-$Ni(OH)_2$ owing to interstratification of the α-motifs in the β-$Ni(OH)_2$ matrix [15]. The peaks of samples S-2 and S-3 (curves b and c) matched well with the nickel nitrate hydroxide standard pattern (JCPDS Card No. 22-752) [16]. On the basis of the general formula of α-$Ni(OH)_2$, $[Ni(OH)_{2-x}A^{n-1}_{x/n} \cdot yH_2O]$ with $x = 0.2–0.4$, $y = 0.6–1$ and $A = Cl^-$, NO^{3-}, CO_3^{2-} or OCN^-, the products were definite α-form. The peaks at 12.2° and 24.7° of samples S-2 and S-3 corresponded to the (001) and (002) planes, respectively. Also, the peaks of the samples S-2 and S-3 obtained a slight shift, which was attributed to the extent and type of the intercalated anions in the $Ni(OH)_2$ lattices. Besides, the peak intensity of sample S-3 is stronger than that of S-2, which may be because of the high filling ratio. After calcinations, all the precursor samples changed into the cubic crystalline structure of NiO (JCPDS Card No. 4-835). Furthermore, with the increasing of calcination temperature, all peaks became sharp with high intensities, which implied that a high crystallinity NiO phase was obtained.

The TG curve of the sample S-1 is shown in Fig. 2*a*. There are three main weight loss regions with a net weight loss of −28%. The initial weight loss of about −3.5% is ascribed to the loss of the surface adsorbed water and ethanol. The second weight loss of about −22% is because of the removal of crystalline water and decomposition of intercalated anions between α-$Ni(OH)_2$, which is larger than the theoretic value (19.4%).

$$Ni(OH)_2 \rightarrow NiO + H_2O \text{ (mass loss 19.4\%)} \quad (1)$$

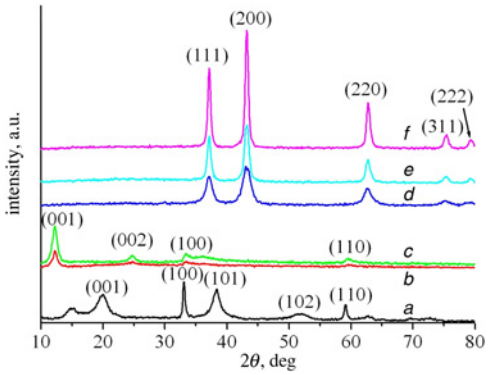

Figure 1 *XRD patterns of as-prepared precursors*
a–c S-1, S-2 and S-3, respectively
NiO obtained by calcining the precursor at
d–f 300, 400 and 500°C, respectively

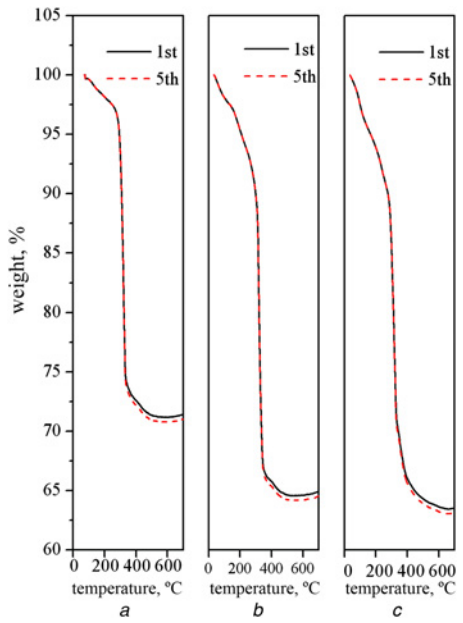

Figure 2 *TG and replicate plots of $Ni(OH)_2$ precursors*
a S-1
b S-2
c S-3, respectively

After 340°C, the weight loss continued but slowed at 400°C and finally ceased at 500°C. The process may be due to the removal of the PEG. As a consequence, the stable residue can be ascribed to NiO.

In contrast, the TG curves of samples S-2 and S-3 both show an increased total weight loss of about −35%. The first weight loss could be because of the removal of the adsorbed water, ethanol and structurally bonded water [17]. The second weight loss of about −23% in the range of 280 and 340°C was because of decomposition of α-$Ni(OH)_2$ and the intercalated anions [18], such as NO_3^-, CO_3^{2-} or OCN^-, which can also demonstrats the formation of α-$Ni(OH)_2$. Then, the decomposition of hydroxides continued up to 450°C to obtain pure NiO (Fig. 1). Furthermore, the replicated results revealed better repeatability (Fig. 2). Fig. 3*a* shows a typical FTIR spectrum of the β-$Ni(OH)_2$ precursor (sample S-1). A narrow and sharp peak at 3641 cm^{-1} is due to the $\upsilon_{O–H}$ stretching vibration, which confirms the brucite structure of the β-$Ni(OH)_2$ phase. Peaks at 3431 and 1618 cm^{-1} are assigned to $\upsilon(H_2O)$ stretching vibration and $\delta(H_2O)$ bending vibration, respectively. The strong band at 521

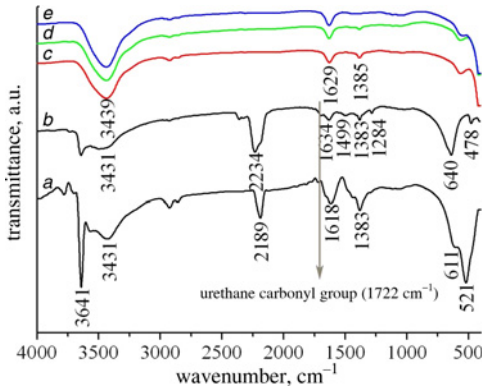

Figure 3 *FTIR spectra of α-$Ni(OH)_2$*
a β-$Ni(OH)_2$
b Precursors and NiO
c–e Obtained by calcining precursors at 300, 400 and 500°C, respectively

doi: 10.1049/mnl.2013.0335

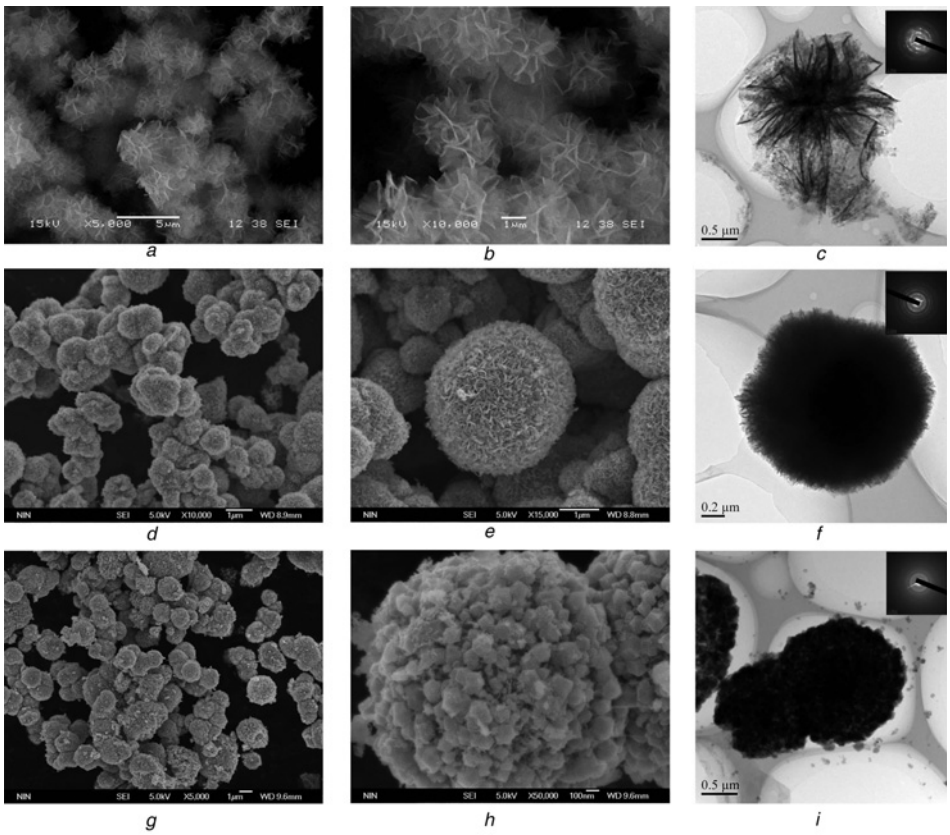

Figure 4 *Typical SEM images of $Ni(OH)_2$ precursors obtained at 160°C for 30 min*
a and *b* Microflowers assembled by nanoleaves (S-1)
d and *e* Walnut-like microspheres (S-2)
g and *h* Particles-aggregated microspheres (S-3)
TEM images (*c*, *f* and *i*) of NiO obtained by calcining corresponding precursors at 400°C for 2 h (inset: the corresponding SAED patterns)

cm^{-1} corresponds to the δ_{O-H} of the hydroxyl group, and the peak at 1383 cm^{-1} was attributed to a trace surface adsorption of nitrate ions [14, 19]. The shoulder peak at about 611 cm^{-1} is due to the stretching vibration of hydroxyl groups hydrogen-boned to Ni–O. In Fig. 3*b*, this spectrum shows typical features of α-$Ni(OH)_2$. The strong absorption bands at 2234, 1499 and 1284 cm^{-1} correspond to the vibration of C ≡ N triple bonds, carbonate ions and nitrate groups, respectively. The bands about 640 and 478 cm^{-1} are because of δ_{OH} and υ_{Ni-OH} vibrations [20]. Curves c–e show the FTIR spectra of calcined products at different temperatures (Fig. 3). With the increasing temperature, the bands about 3439 and 1629 cm^{-1} decreased. The nitrate group related band of about 1385 cm^{-1} decreased to the point of vanishing at 500°C, whereas the increasing band at 400 cm^{-1} proved the formation of NiO species. Besides, the bands at 1722 cm^{-1} were ascribed to the urethane carbonyl groups of PEG [21].

Fig. 4 presents detailed morphologies of the samples. Figs. 4*a* and *b* show the low- and high-magnification FE-SEM images of sample S-1, respectively. It can been seen that the products are mainly composed of large quantities of uniform flower-like microspheres with sizes of 2.0–3.0 μm, whereas the thickness of assembled nanosheets is 10–20 nm. Fig. 4*d* shows the low-magnification FE-SEM image of sample S-2, which consists of monodispersed microspheres with sizes of 2.0–6.0 μm. As shown in Fig. 4*e*, the high-magnification FE-SEM image indicates that a walnut-like α-$Ni(OH)_2$ microsphere was constructed with densely stacked lamellar sheets. Figs. 4*g* and *h* show that the particle-aggregated sample S-3 is composed of smaller 3D nanoparticles with a diameter less than 100 nm. Figs. 4*c*, *f* and *i* are TEM images of NiO obtained by calcined S-1, S-2 and S-3 at 400°C for 2 h, respectively; they possess the same morphology as their corresponding precursors. Besides, the corresponding selected area diffraction (SAED) patterns of the samples (insets in Figs. 4*c*, *f* and *i*) indicated that the calcined products were all polycrystalline.

Fig. 5 shows the cyclic voltammograms (CVs) of different electrodes in 0.1 M PBS with pH 7.0 at a scan rate of 0.1 V s^{-1}. The responses of Hb to NiO/IL/Hb-CPEs were obvious and their reversibility are all favourable. The F-NiO/IL/Hb-CPE (curve a) was especially favourable, in which a pair of stable and well-defined redox peaks appeared with an anodic peak potential (E_p, a) of −0.230 V, a cathodic peak potential (E_p, c) of −0.319 V and ΔE_p of 0.089 V, suggesting a fast and quasi-reversible electron transfer process. The apparent formal potential ($E0'$), which is defined as the average value of the E_p, c and E_p, a, was estimated to be −0.275 V,

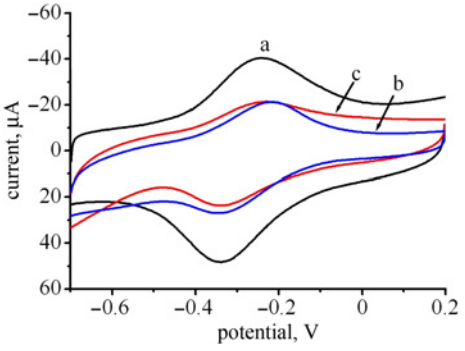

Figure 5 *CV of a F-NiO/IL/Hb-CPE, b W-NiO/IL/Hb-CPE, c A-NiO/IL/Hb-CPE*
Supporting solution: 0.1 M pH 7.0 PBS, scan rate: 0.1 V s^{-1}

which was characteristic of the reversible electrode process of the heme Fe(III)/Fe(II) couples in the immobilised Hb. From the comparison of electrochemical behaviour of Hb with different modified electrodes, it is clear that NiO played an important role in facilitating the direct electron transfer between Hb and the underlying electrode by the synergetic effect with BmimBr. The reason for this could be as follows. The good biocompatibility of the NiO/IL composite may have prevented denaturation and retains the essential secondary structure of the entrapped protein. More importantly, the flower-like architecture of F-NiO was accessible for Hb molecules to enter into the inside of the F-NiO microspheres, and more Hb molecules were aggregated onto the nanopetal surfaces. Moreover, F-NiO was abundant in active sites for protein binding and could act as a rigid framework to encourage the appropriate conformation of entrapped proteins, facilitating the direct electron transfer between the redox proteins and the underlying electrode. Furthermore, the film composed of water-miscible BmimBr and electric NiO exhibited excellent conductivity and also contributed to the efficient electron transfer. Compared with F-NiO/IL/Hb-CPE, the peak currents of W- and A-NiO/IL/Hb-CPE were decreased, which might be because of the structurally different NiO materials. The small cavities and uniform structures on the surface of W-NiO and A-NiO limited the Hb to only being adsorbed on the surface of the microspheres.

4. Conclusions: In summary, $Ni(OH)_2$ microspheres with different morphologies, including flower-like, walnut-like and particles aggregated into microspheres, have been synthesised successfully via a surfactant-assisted microwave hydrothermal method. The as-calcined NiO microspheres were also well preserved with the same morphologies as their corresponding precursors. The surfactant with different molecular weight and filling ratio in the hydrothermal process would have an important effect on controlling the morphology of the Ni-based microspheres. The electrochemical test results showed that NiO/IL/HB-CPEs were suitable for the detection of haemoglobin, however the detection sensitivity and reversibility of the electrodes is different because of the various morphologies of NiO. These $Ni(OH)_2$ and NiO materials with different morphologies could be used in chemical sensors, catalysts, fuel cell electrodes and so on.

5. Acknowledgments: The authors acknowledge financial support from the National Natural Science Foundation of China (51272147), the Special Fund from the Shaanxi Provincial Department of Education (12JK0467) and the Graduate Innovation Fund of Shaanxi University of Science and Technology.

6 References

[1] Ovshinsky S.R., Fetcenko M.A., Ross J.: 'A nickel metal hydride battery for electric vehicles', *Science*, 1993, **260**, (5105), pp. 176–181
[2] Mavis B., Akine M.: 'Three-component layer double hydroxides by urea precipitation: structural stability and electrochemistry', *J. Power Sources*, 2004, **134**, (2), pp. 308–317
[3] Dirksen J.A., Duval K., Ring T.A.: 'NiO thin-film formaldehyde gas sensor', *Sens. Actuators B*, 2001, **80**, (2), pp. 106–115
[4] Kawano M., Yoshida H., Hashino K., *ET AL.*: 'Synthesis of matrix-type NiO–SDC composite particles by spray pyrolysis with acid addition for development of SOFC cermet anode', *J. Power Sources*, 2007, **173**, (1), pp. 45–52
[5] Wang D., Xu R., Wang X., Li Y.: 'NiO nanorings and their unexpected catalytic property for CO oxidation', *Nanotechnology*, 2006, **17**, pp. 979–982
[6] Chen J., Bradhurst D.H., Dou S.X., Liu H.K.: 'Nickel hydroxide as an active material for the positive electrode in rechargeable alkaline batteries', *J. Electrochem. Soc.*, 1999, **146**, (10), pp. 3606–3612
[7] Sun Y., Xia Y.: 'Shape-controlled synthesis of gold and silver nanoparticles', *Science*, 2002, **298**, (5601), pp. 2176–2179
[8] Peng Z.A., Peng X.: 'Nearly monodisperse and shape-controlled CdSe nanocrystals via alternative routes: nucleation and growth', *J. Am. Chem. Soc.*, 2002, **124**, (13), pp. 3343–3353
[9] Yin Y.D., Alivisatos A.P.: 'Colloidal nanocrystal synthesis and the organic–inorganic interface', *Nature*, 2005, **437**, (7059), pp. 664–670
[10] Wang X., Zhuang J., Peng Q., Li Y.D.: 'A general strategy for nanocrystal synthesis', *Nature*, 2005, **437**, (7055), pp. 121–124
[11] Wu C.Z., Lei L.Y., Zhu X., Yang J.L., Xie Y.: 'Large-scale synthesis of titanate and anatase tubular hierarchitectures', *Small*, 2007, **3**, (9), pp. 1518–1522
[12] Shang M., Wang W.Z., Zhang L., Sun S.M., Wang L., Zhou L.: '3D Bi_2WO_6/TiO_2 hierarchical heterostructure: controllable synthesis and enhanced visible photocatalytic degradation performances', *J. Phys. Chem. C*, 2009, **113**, (13), pp. 14727–14731
[13] Kim T., Lian J.B., Ma J.M., Duan X.C., Zheng W.J.: 'Morphology controllable synthesis of γ-alumina nanostructures via an ionic liquid-assisted hydrothermal route', *Cryst. Growth Des.*, 2010, **10**, (7), pp. 2928–2933
[14] Xu L.P., Ding Y.S., Chen C.H., *ET AL.*: '3D flowerlike α-nickel hydroxide with enhanced electrochemical activity synthesized by microwave-assisted hydrothermal method', *Chem. Mater.*, 2008, **20**, (1), pp. 308–316
[15] Ramesh T.N., Kamath P.V.: 'Synthesis of nickel hydroxide: effect of precipitation conditions on phase selectivity and structural disorder', *J. Power Sources*, 2006, **156**, (2), pp. 655–661
[16] Rajamathi M., Kamath P.V.: 'On the relationship between α-nickel hydroxide and the basic salts of nickel', *J. Power Sci.*, 1998, **70**, (1), pp. 118–121
[17] Zhou Y.L., Wang J.M., Chen H., Pan T., Zhang J.Q., Caom C.N.: 'Al-substituted α-nickel hydroxide prepared by homogeneous precipitation method with urea', *Int. J. Hydrog. Energy*, 2004, **29**, (8), pp. 889–896
[18] Xu Z.P., Zeng H.C.: 'Abrupt structural transformation in hydrotalcite-like compounds $Mg_{1-x}Al_x(OH)_2(NO_3)_x{\cdot}nH_2O$ as a continuous function of nitrate anions', *J. Phys. Chem. B*, 2001, **105**, (9), pp. 1743–1749
[19] Xu Z.P., Xu R., Zeng H.C.: 'Sulphate-functionaled carbon/metal-oxide nanocomposites from hydrotalcite-like compounds', *Nano Lett.*, 2001, **1**, (3), pp. 703–706
[20] Jeevanandam P., Koltypin Y., Gedanken A.: 'Synthesis of nanosized α-nickel hydroxide by a sonochemical method', *Nano Lett.*, 2001, **1**, (5), pp. 263–266
[21] Oh C., Ki C.D., Chang J.Y., Oh S.G.: 'Preparation of PEG-grafted silica particles using emulsion method', *Mater. Lett.*, 2005, **59**, (8–9), pp. 929–933

doi: 10.1049/mnl.2013.0335